

# Nanostructured optical waveguide with a highly confined mode

EUGENY D. CHUBCHEV,<sup>1,\*</sup> IGOR A. NECHEPURENKO,<sup>1,2</sup> ALEXANDER V. DOROFEENKO,<sup>1,2,3,4</sup>  ALEXEY P. VINOGRADOV,<sup>1,3,4</sup> AND ALEXANDER A. LISYANSKY<sup>5,6</sup>

<sup>1</sup>Dukhov Research Institute of Automatics (VNIIA), 22 Sushchevskaya, Moscow 127055, Russia

<sup>2</sup>Kotel'nikov Institute of Radioengineering and Electronics of Russian Academy of Sciences, Mokhovaya 11-7, Moscow 125009, Russia

<sup>3</sup>Institute for Theoretical and Applied Electromagnetics of Russian Academy of Sciences, 13 Izhorskaya, Moscow 125412, Russia

<sup>4</sup>Moscow Institute of Physics and Technology, Dolgoprudny, Moscow Region 141700, Russia

<sup>5</sup>Department of Physics, Queens College of the City University of New York, Queens, New York 11367, USA

<sup>6</sup>The Graduate Center of the City University of New York, New York, New York 10016, USA

\*Corresponding author: eugene.chubchev@yandex.ru

Received 4 May 2020; revised 21 July 2020; accepted 21 July 2020; posted 22 July 2020 (Doc. ID 396739); published 18 August 2020

**We propose a transmission line working at telecom wavelengths with a cross section as small as  $\lambda^2/39$ , which is 1.6 times smaller than that of an optimized silicon waveguide. The proposed line can be implemented as a subwavelength fiber with plasmonic cladding. This considerable decrease in the line cross section is achieved by utilizing a plasmonic quasi-antisymmetric mode. The required plasmonic cladding is rather thin; therefore, losses are moderate and could be compensated by using amplifying core materials. Such a transmission line can find applications in densely integrated optical systems.** © 2020 Optical Society of America

<https://doi.org/10.1364/JOSAB.396739>

## 1. INTRODUCTION

The development of modern information technologies requires increasing the clock frequency, preferably up to the optical frequencies, and reducing the mode area of transmission lines. To achieve these goals, one requires materials that allow for strong mode confinement and long propagation length. Conventional circuits for direct or alternative currents, as well as for transmission lines operating at radio and microwave frequencies, are usually made of high conducting metals. To minimize loss, the thickness,  $\delta_s$ , of the skin layer should be smaller than the thickness,  $L_m$ , of metal elements. To achieve a subwavelength cross section of a transmission line,  $L_m$  must be much smaller than the free-space wavelength  $\lambda_0$ . Thus, for a small cross section and a long propagation length, one needs  $\lambda_0 \gg L_m \gg \delta_s$ . These inequalities are easily satisfied at frequencies up to several GHz. For this frequency range, many transmission lines with small cross sections have been designed. An example of such a line is a two-wire circuit and a coaxial line.

At optical frequencies, metals are not good conductors; their skin depth is not very small (e.g., 20–30 nm for silver). Although the optical hybrid waveguide suggested in [1], which localizes a mode between a GaAs cylinder and a silver substrate, has an acceptable mode area of  $\sim 10^{-3}\lambda_0^2$ , the size of auxiliary elements (the cylinder and a nearby part of the substrate) of the transmission line makes the total cross section of the line about  $(\lambda_0/3)^2$ . For this reason, such lines should be placed at a

distance larger than that derived from the mode area, since this distance is determined by the waveguide geometry. Namely, the diameter of the high-permittivity cylinder is about 400 nm, which is comparable to the typical size of a silicon waveguide [2]. Therefore, further decrease in the waveguide cross section is still desirable.

Another approach to create an optical transmission line uses the effect of total internal reflection. Transmission lines utilizing this effect are known as optical fibers [3–5]. At the telecommunication frequencies, the diameter of such waveguides is dozens of micrometers. In the surrounding medium (vacuum), the characteristic length scale of confinement of modes traveling along a waveguide with the cylindrical symmetry is determined by the imaginary part of the transverse wave number of the mode,  $\kappa = \sqrt{k_z^2 - k_0^2}$ , where  $k_0$  is the free-space wavenumber and  $k_z$  is the propagation constant. Consequently, the mode area,  $S_{\text{mode}}$ , which is defined as in Ref. [1] (see also Section 2), is estimated as  $S_{\text{mode}} \sim 1/\kappa^2$ . Making the cross section of the waveguide smaller than  $(\lambda_0/\sqrt{\epsilon})^2$  results in  $k_z$  approaching  $k_0$ , while  $S_{\text{mode}} \sim 1/\kappa^2 \rightarrow \infty$ .

Noticeable confinement can be achieved far from the light cone,  $k_z \gg k_0$ . However, even in this case, the mode area is too large because applications require optical waveguide modes with a transverse size comparable to the sizes of electronic components (dozens of nanometers) [5,6]. The transverse size of a waveguide could be decreased by using high-permittivity

materials [5]. Unfortunately, there are no transparent dielectric materials with permittivity greater than 12 in optics and at near IR [7], which is not sufficient for an acceptable reduction of the waveguide cross section [5,8–11].

At telecom frequencies the plasmonic materials have high values of permittivity and, it has been suggested, several plasmonic waveguides [12–24]. Unfortunately, due to losses purely plasmonic waveguides, however, cannot have both a large propagation length and a small mode area.

Nevertheless, it seems that the only way out is using a combination of plasmonic and dielectric materials, which allows the increase of the propagation length at a subwavelength mode area. Adding a plasmonic cladding to a dielectric waveguide leads to an appearance of two more plasmonic modes classified as  $HE_1$  [22]. Plasmonic modes are generally distinguished by the distributions of the magnetic field in the cladding [25]. According to this classification, the  $HE_1$  modes are referred to as quasi-symmetric and quasi-antisymmetric. In the case of the thick cladding studied in Ref. [22], the quasi-antisymmetric mode is similar to the channel mode in bulk metal, while the quasi-symmetric mode resembles the mode of a metal cylinder. In the visible range, the quasi-symmetric mode has a high loss that hinders its use. Therefore, in Ref. [22], the attention was focused on the quasi-antisymmetric  $HE_1$  mode, which is localized outside the waveguide and has lower loss. The mode area of quasi-symmetric  $HE_1$  mode diverges as the waveguide cross section vanishes. This mode, therefore, is not acceptable for designing optical transmission lines with subwavelength mode area.

In this paper, we study the quasi-antisymmetric  $HE_1$  mode at the telecommunications wavelength  $\lambda_0 = 1550$  nm. We show that the area of this mode decreases with a decrease in the waveguide cross section. This possibility occurs because there is an interval of the waveguide radii, at which the Hashin–Shtrikman condition [26–28] for mutual subtraction of the transverse polarizations of the cladding and core is almost realized. Consequently, the fields outside the waveguide are small, and the mode area reduces to the cross section of the core. In the proposed waveguide, both the mode area and the cross section of the line are much smaller than  $\lambda_0^2$ . At a small thickness of the metal cladding, the mode may have a propagation length of 10  $\mu\text{m}$ . It is sufficient for using it in small optic-based chips with THz clock frequency. To achieve larger propagation lengths, gain materials with high gain factors should be implemented. We show that loss compensation for the quasi-antisymmetric  $HE_1$  mode is possible with the use of semiconductor materials even at subwavelength mode cross section.

## 2. WAVEGUIDE MODE OF SUBWAVELENGTH AREA

We consider the transmission properties of a waveguide consisting of a core of a subwavelength radius  $a$  and permittivity  $\varepsilon_{\text{in}}$  covered with a cladding of a subwavelength thickness  $d_{\text{cladd}}$  and permittivity  $\varepsilon_{\text{cladd}}$  (see inset in Fig. 1). The system is surrounded by a vacuum (permittivity  $\varepsilon_{\text{out}} = 1$ ). We deal with the quasi-antisymmetric  $HE_1$  mode that exists above the threshold determined by  $k_0 a \sqrt{\varepsilon_{\text{in}}} \sim 1$ . For the telecommunication frequencies, this condition is realized in silver, in which the real

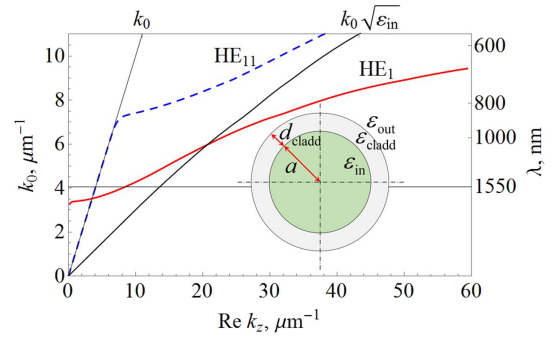


**Fig. 1.** Dispersion curves for the two lowest modes in the waveguide with a core radius of 120 nm core and a cladding thickness of 20 nm. Straight lines show the light lines for the vacuum ( $k_0 = k_z$ ) and the core material ( $k_0 = k_z / \sqrt{\varepsilon_{\text{in}}}$ ). Solid red and dashed blue curves correspond to  $HE_1$  (quasi-antisymmetric in metal) and  $HE_{11}$  modes, respectively. The permittivity dispersions of GaAs and Ag are taken from Refs. [29,30].

part of the permittivity of the cladding is negative ( $\varepsilon'_{\text{cladd}} \ll -1$ ) [25]. In this mode, the field concentrates inside the core [22].

We consider the wavelength of  $\lambda_0 = 1550$  nm. The values of  $d_{\text{cladd}}$  are chosen to be smaller or equal to the silver skin depth, which is about 30 nm [15]. To begin with, we assume that  $a = 120$  nm and  $d_{\text{cladd}} = 20$  nm. The dielectric constant of the core is  $\varepsilon_{\text{in}} = 11$ . The cladding material is silver, for which permittivity at  $\lambda_0$  is  $-129 + 3.28i$  [29]. The wavenumber  $k_z$  of the quasi-antisymmetric plasmon exceeds  $k_0$  (Fig. 1, the intersection of the red solid dispersion curve with the horizontal line corresponding to  $\lambda_0 = 1550$  nm). At this wavelength, the waveguide is practically single mode, because the quasi-symmetric  $HE_1$  plasmonic mode appears at higher frequencies at the UV range (not shown in Fig. 1). The  $HE_{11}$  mode is extremely close to the light cone (dashed blue curve in Fig. 1) and almost transforms into a plane wave. It has a mode area much larger than  $\lambda_0^2$ . The ratio of mode areas for  $HE_{11}$  and  $HE_1$  modes is of the order of  $10^7$ . In fact, a mode with so high a mode area can hardly be considered as a guided mode.

Due to cylindrical symmetry, all of the mode components depend on the azimuthal angle  $\varphi$  as  $\exp[i m \varphi]$ , where  $m$  is the mode azimuthal number. Throughout this paper, we suppose  $m = 1$ . In [9], it is shown that the components of the electric,  $\mathbf{E}$ , and magnetic,  $\mathbf{H}$ , fields of the  $HE_1$  mode outside of the waveguide are determined by the following equations:

$$\begin{aligned} E_r^{(\text{out})} &= -\frac{1}{\kappa^2} \left( i k_z C_E \frac{\partial}{\partial r} - \frac{k_0}{r} C_H \right) \frac{K_1(\kappa r)}{K_1(\kappa b)} \exp(i k_z z + i \varphi), \\ E_\varphi^{(\text{out})} &= -\frac{1}{\kappa^2} \left( -i k_0 C_H \frac{\partial}{\partial r} - \frac{k_z}{r} C_E \right) \frac{K_1(\kappa r)}{K_1(\kappa b)} \exp(i k_z z + i \varphi), \\ E_z^{(\text{out})} &= C_E K_1(\kappa r) / K_1(\kappa b) \exp(i k_z z + i \varphi), \\ H_r^{(\text{out})} &= -\frac{1}{\kappa^2} \left( \varepsilon_{\text{out}} \frac{k_0}{r} C_E + i k_z C_H \frac{\partial}{\partial r} \right) \frac{K_1(\kappa r)}{K_1(\kappa b)} \exp(i k_z z + i \varphi), \\ H_\varphi^{(\text{out})} &= -\frac{1}{\kappa^2} \left( i k_0 \varepsilon_{\text{out}} C_E \frac{\partial}{\partial r} - \frac{k_z}{r} C_H \right) \frac{K_1(\kappa r)}{K_1(\kappa b)} \exp(i k_z z + i \varphi), \\ H_z^{(\text{out})} &= C_H K_1(\kappa r) / K_1(\kappa b) \exp(i k_z z + i \varphi), \end{aligned} \quad (1)$$

where  $b = a + d_{\text{cladd}}$  is the external radius of the waveguide,  $\varepsilon_{\text{in}}$  is the permittivity of the waveguide core, and  $K_1$  is the modified Bessel function of the second kind.  $C_E$  and  $C_H$  are equal to the amplitudes of longitudinal field components  $E_z^{(\text{out})}$  and

$H_z^{(\text{out})}$  at the outer waveguide boundary [9,31]. Note that the derivatives over  $\varphi$  are taken explicitly as  $\partial/\partial\varphi = i$ . The relation between  $C_E$  and  $C_H$  is found from the boundary conditions at  $r = a$  and  $r = b$ . The absolute values of  $C_E$  and  $C_H$  are normalized by the condition  $\max\left(\frac{\partial(\varepsilon\omega)}{\partial\omega}|\mathbf{E}|^2 + |\mathbf{H}|^2\right) = 1$ . The equations for the fields inside the core and the cladding are provided in Supplement 1.

Since we are interested in the modes with the subwavelength mode area, we have to choose both the core radius and the cladding thickness to be smaller than the free-space wavelength ( $k_0a \ll 1$  and  $k_0d_{\text{cladd}} \ll 1$ ). Therefore, in the neighborhood of the core-cladding waveguide, a near-field region  $k_0r \ll 1$  appears. We deal with the values of  $k_z$ , which are only slightly larger than those of  $k_0$ . This means that in the near-field region, the inequality  $\kappa \ll k_0$  holds, resulting in  $\kappa r \ll 1$ . Then, in Eq. (1), the functions  $K_1(\kappa r)$  may be expanded in the power series

$$K_1(\kappa r) \approx 1/(\kappa r) + (2\gamma - 1)\kappa r/4 + (\kappa r/2) \ln(\kappa r/2) + O((\kappa r)^2), \quad (2)$$

where  $\gamma$  is the Euler constant.

First, for  $\kappa r \ll 1$ , in Eq. (2), we can retain only the first term,  $K_1(\kappa r) \approx 1/(\kappa r)$ . In this approximation, the derivative  $\partial/\partial r$  can be replaced with  $-1/r$ , and the first equation in Eq. (1) is reduced to

$$E_r^{(\text{out})} = (ik_z C_E + k_0 C_H) \frac{b}{\kappa^2 r^2} \exp(ik_z z + i\varphi). \quad (3)$$

The other field components are reduced in the same manner.

Finally, the near-field contribution outside the core and cladding into the mode area,  $S_{\text{mode}} = 2\pi \int_0^{+\infty} (|\mathbf{E}|^2 + |\mathbf{H}|^2) r dr$ , may be estimated as

$$S_{\text{NF}} \sim \int_b^{+\infty} |E_r^{(\text{out})}|^2 r dr = \frac{1}{\kappa^4} |ik_z C_E + k_0 C_H|^2 b^2 \times \int_b^{+\infty} \frac{dr}{r^3} \sim \frac{1}{\kappa^4} |ik_z C_E + k_0 C_H|^2. \quad (4)$$

In the far-field region,  $\kappa r \gg 1$ ,  $K_1(\kappa r) \approx \sqrt{\pi/2\kappa r} \exp(-\kappa r)$ . Then, from Eq. (1) we obtain

$$E_r^{(\text{out})} \sim \frac{ik_z C_E}{\kappa} \sqrt{\frac{b}{r}} \exp(-\kappa r), \quad (5)$$

and the far-field contribution into the mode area results in

$$S_{\text{FF}} \sim \int_{1/\kappa}^{+\infty} |E_r^{(\text{out})}|^2 r dr \approx \frac{b k_z^2}{2\kappa^3} |C_E|^2 e^{-2}.$$

High confinement requires that  $S_{\text{NF}} \gg S_{\text{FF}}$ . Then,  $S_{\text{mode}}$  is determined by  $S_{\text{NF}}$  only, and we obtain the condition for the subwavelength mode area

$$b \ll e^2 \frac{|n_z C_E - i C_H|^2}{\kappa |C_E|^2}. \quad (6)$$

Under this condition, the field is localized at a length scale much smaller than  $1/\kappa$ . Since at such distances the field decreases considerably, the mode confinement in the suggested waveguide does not require large wavenumbers, as is usually believed. In Fig. 2, the distributions of the  $z$ -component of Poynting vector  $S_z$  calculated in COMSOL Multiphysics is shown. Comparing these distributions for different system parameters, we can see that the subwavelength mode confinement can be obtained in a broad range of parameters. The key moment is that the mode area is formed in the near-field region

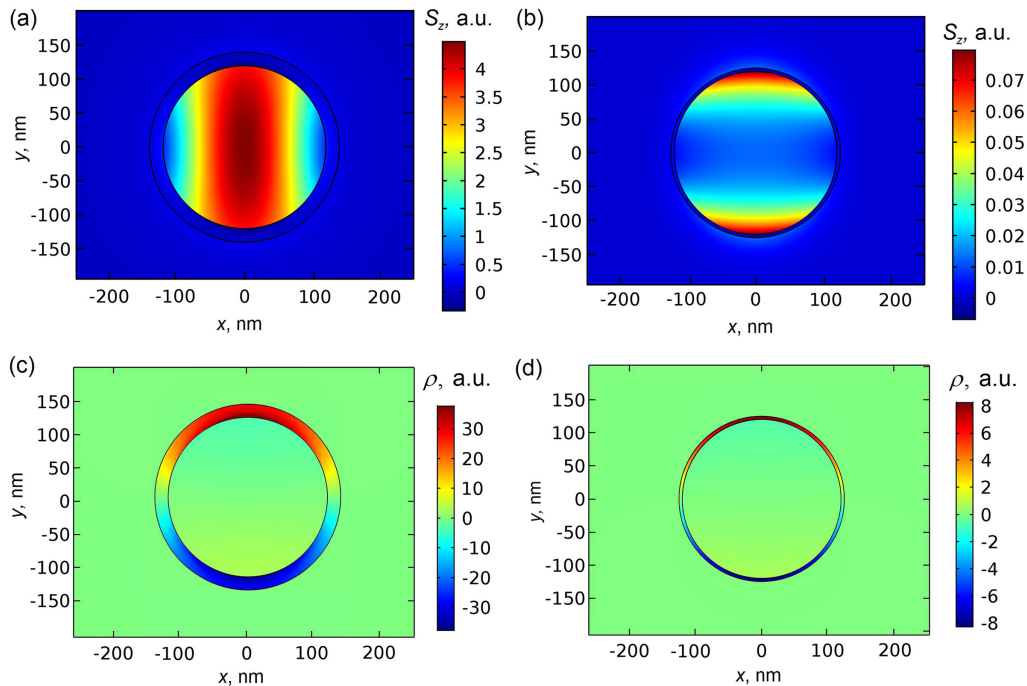


**Fig. 2.** Distribution of the  $z$ -component of Poynting vector (a), (b) and of the charge density (c), (d) of the mode at (a), (c)  $a = 120$  nm and  $d_{\text{cladd}} = 20$  nm, and (b), (d)  $a = 120$  nm and  $d_{\text{cladd}} = 5$  nm. The corresponding values of the propagation constant are  $k_z = (2.01 + 0.029i)k_0$  for (a), (c) and  $k_z = (4.46 + 0.09i)k_0$  (b), (d).

of the waveguide. The contribution of the far-field region decays exponentially and is negligibly small (see Fig. 2). Despite the difference in the field distribution, the charge density distribution is quite similar in both cases [Figs. 2(c) and 2(d)]. In the quasi-antisymmetric  $HE_1$  mode, a charge density distribution is quasi-symmetric, i.e., the charge has the same sign across the metal film. Such charge distribution is observed for both examples in Figs. 2(c) and 2(d), which confirms that the same mode is shown. On the other hand, a charge density distribution of the quasi-symmetric  $HE_1$  mode is quasi-antisymmetric, i.e., the charge changes the sign across the metal film (see Refs. [25,32] for more details). It should be noted that, instead of  $\exp(\pm i\varphi)$ , the  $\cos(\varphi)$  dependence of  $S_z$  is shown in Fig. 2.

The reason for the field suppression outside the waveguide is the Hashin-Shtrikman effect of the dielectric dipole moment compensation by a metallic cladding, which leads to the field concentration inside the core.

In order to show that the subwavelength mode confinement can be obtained in a wide range of parameters, we show the mode area as a function of the core radius  $a$  and the cladding thickness  $d_{\text{cladd}}$  (see Fig. 3). The mode area is calculated via the equation  $S_{\text{mode}} = 2\pi \int_0^{+\infty} \left( \frac{\partial(\varepsilon\omega)}{\partial\omega} |\mathbf{E}|^2 + |\mathbf{H}|^2 \right) r dr$  with the normalization condition  $\max\left(\frac{\partial(\varepsilon\omega)}{\partial\omega} |\mathbf{E}|^2 + |\mathbf{H}|^2\right) = 1$ .

It should be noted that the mode area  $S_{\text{mode}}$  can take values less than  $\pi(a + d_{\text{cladd}})^2$ . The reason for this is a concentration of the field in some part of the waveguide core. Inside the waveguide core, the fields are expressed via the Bessel function,  $J_1(\sqrt{\varepsilon_{\text{in}}k_0^2 - k_z^2}r)$ , and its derivatives. These functions oscillate at  $n_z < \sqrt{\varepsilon_{\text{in}}}$ , and the field intensity has a maximum in the center of the core. On the other hand, at  $n_z \gg \sqrt{\varepsilon_{\text{in}}}$  and  $k_z a \gg 1$ , the Bessel function decays into the core,  $J_1(\sqrt{\varepsilon_{\text{in}}k_0^2 - k_z^2}r) \sim \exp(\sqrt{k_z^2 - \varepsilon_{\text{in}}k_0^2}r)$ , so that the field is concentrated in the cladding. This leads to a significant reduction of the  $S_{\text{mode}}$  below the waveguide cross-section  $\pi a^2$  at small values of  $d_{\text{cladd}}$  (see Fig. 4).

### 3. COMPENSATION FOR LOSSES

Since in the optical region, all the plasmonic metals have significant Joule losses, the propagation length of the waveguide mode

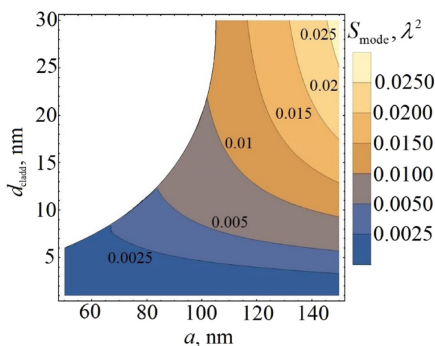


**Fig. 3.** Mode area as a function of the waveguide radius  $a$  and the cladding thickness  $d_{\text{cladd}}$ . In the white area, the mode is leaky. The boundary of the white region corresponds to the cutoff where  $k_z$  approaches  $k_0$ . The value of  $1/\kappa$  grows near the boundary; however, the mode area stays deeply subwavelength as has been discussed above.

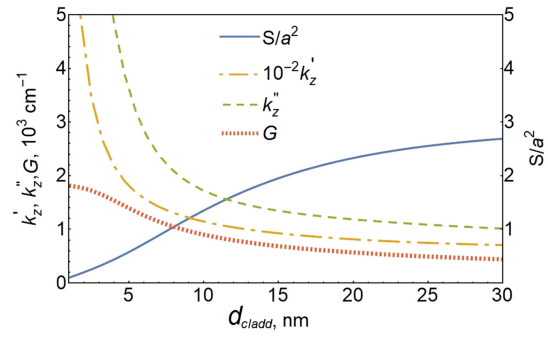


**Fig. 4.** Mode area  $S_{\text{mode}}$  (the solid line), the real (the dash-dotted yellow line) and imaginary (the dashed green line) parts of  $k_z$ , and the material gain  $G$  required for loss compensation (the red dotted line) as a function of the cladding thickness  $d_{\text{cladd}}$  at radius  $a = 120$  nm.

is not large. In Fig. 5(a), the propagation length  $l_{\text{pr}} = 1/(2\text{Im}k_z)$  is shown as a function of  $a$  and  $d_{\text{cladd}}$ . For the waveguide with the core radius of 120 nm and the cladding thickness of 20 nm, the mode propagation length is equal to  $l_{\text{pr}} = 4.2 \mu\text{m}$ , which is sufficient for future applications. Note that when the cladding thickness decreases, the volume occupied by the metal also decreases. Nevertheless, due to the field concentration in the metallic cladding in the electrostatic regime, losses increase.

Energy absorption can be fully compensated if the waveguide core is made of a gain medium, such as quantum dots [33,34], quantum wells [35], or nanorods [36]. However, even these strong gain media are not sufficient for loss compensation in the most plasmonic geometries. In our system, loss compensation is the most possible due to the small metal cladding thickness compared to the waveguide core [37]. Since the mode energy is mainly concentrated inside the core (see Fig. 2), gain should be localized in the same region. In the proposed waveguide, loss compensation can be achieved at realistic values of material gain. Figure 5(b) shows the material gain sufficient for loss compensation as a function of  $a$  and  $d_{\text{cladd}}$ . We consider the core made of a GaAsBi/GaAs nanowire. Such quantum wells have the material gain of approximately  $1500 \text{ cm}^{-1}$  [38] and permittivity  $\varepsilon'_{\text{in}} = 11$  [39].

To calculate the material gain  $G$  required for loss compensation, we numerically solve the dispersion equation. We find an imaginary part of the core permittivity,  $\varepsilon''_{\text{in}}$ , which provides purely real values of  $k_z$ . The value of  $G$  is calculated via the equation  $G = -\text{Im}\sqrt{\varepsilon'_{\text{in}} + i\varepsilon''_{\text{in}}k_0}$ . As shown in Fig. 5(b), the material gain sufficient to compensate the absorption is of the order of  $1000 \text{ cm}^{-1}$ , which is achievable employing GaAs nanowires [40]. In particular, the material gain required for loss compensation in a waveguide with the core radius of  $a = 120$  nm and the cladding thickness of  $d_{\text{cladd}} = 20$  nm is  $568 \text{ cm}^{-1}$  at  $1550$  nm.

In many cases, to increase the propagation length, a partial loss compensation may be sufficient. With the help of the data for  $k_z''$  in a system without gain and for the gain  $G$  that provides the total loss compensation (dotted and dashed curves in Fig. 4), one can estimate the mode propagation length at any intermediate gain level  $g$  ( $0 < g < G$ ). To do this, let us note that the difference between the material gain  $G$  and the modal loss  $k_z''$  is due to the field distribution both inside and

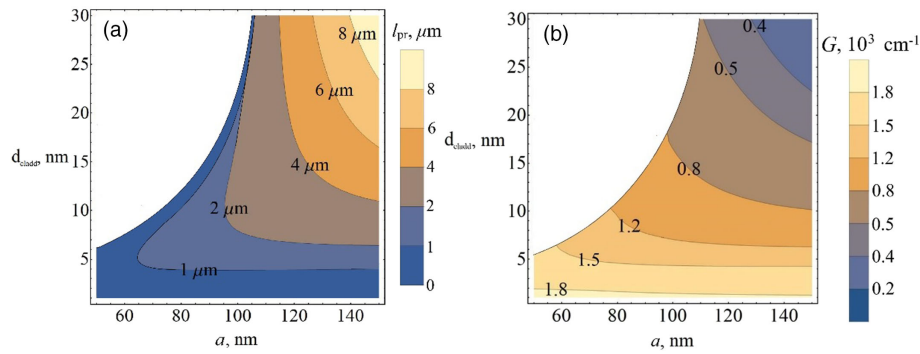


**Fig. 5.** Propagation length (a) and the value of material gain required for loss compensation (b) versus the radius of the waveguide and the thickness of the cladding. In the white area, the mode is leaky.

outside the gain medium. Let us suppose that the field fraction located in the gain medium does not depend on the gain level. Therefore, at an arbitrary gain level, the imaginary part of the wavenumber at a current level of gain,  $k_z''(g)$ , is a difference of its value without gain,  $k_z'' = k_z''(0)$ , and of the term caused by gain:  $k_z''(g) = k_z'' - \chi g$ . Here, the coefficient  $\chi$  is calculated from the total gain compensation:  $0 = k_z'' - \chi G$ . Thus, one obtains  $k_z''(g) = k_z'' - k_z'' g/G$ , and the propagation length  $L(g) = 1/2k_z''(g)$  is estimated as

$$l_{pr}(g) = \frac{l_{pr}(0)}{1 - g/G}, \quad (7)$$

or  $l_{pr}(g) = l_{pr}(0)G/(G - g)$ . Particularly, for  $l_{pr}(0) = 4.2 \mu\text{m}$  and  $G = 568 \text{ cm}^{-1}$ , the value of gain  $g = 330 \text{ cm}^{-1}$  increases the propagation length up to  $l_{pr}(g) = 10 \mu\text{m}$ .

#### 4. CONCLUSION

We study a structure of an optical dielectric waveguide with a thin metal cladding. We demonstrate that utilizing the quasi-antisymmetric mode  $\text{HE}_1$  allows one to construct a transmission line with a subwavelength cross section and a sufficiently long propagation length of  $4.2 \mu\text{m}$ , which is enough for communication between the usual (electronic) kernels. In a subwavelength neighborhood of the waveguide, the electromagnetic field acquires a near-field character. This special property is accompanied by a power-law decay in 2D and 3D systems (cladding fiber and chain of spherical particles), and cannot be realized in layered systems in which there is no near-field decay. The contribution of the near-field region is crucial in the formation of the area of the mode propagating along the waveguide. Upon exiting this region, the field acquires a far-field character. In the far-field region, the field decays exponentially,  $\sim \exp(-\kappa r)$ , but with a very small decay rate,  $\kappa = \sqrt{k_z^2 - k_0^2}$  with  $k_z \sim k_0$ . Therefore, strong decay in the near field makes the contribution of the far-field negligible, so that the mode area is  $S_{\text{mode}} \ll 1/\kappa^2$ .

In Ref. [21], a transmission line operating in the quasi-symmetric mode was considered in the visible range. Although this transmission line realization has a cross section of  $(\lambda_0/3)^2$ , the mode area is determined by the same relation as discussed above,  $S_{\text{mode}} \sim 1/\kappa^2$ . Due to a high loss in metal, the possible

values of  $k_z$  are about  $k_0$  [15,41,42], which do not allow for the subwavelength confinement of the mode [43].

The range of geometrical and material parameters needed for the realization of the proposed waveguide is shown in Fig. 3. A mode area as small as  $0.01\lambda^2$  at  $\lambda = 1550 \text{ nm}$  is achievable even if the mode wavenumber is only slightly larger than the free-space wavenumber. Due to the thin cladding, Joule losses in metal can be compensated if the core of the waveguide is made of a gain medium such as quantum dots, quantum wells, or nanorods. The proposed waveguide can find applications in dense integrated optical circuits and crosstalk suppression.

**Funding.** Office of Naval Research (N00014-20-1-2198).

**Acknowledgment.** We are thankful to Oleg Kotov and Sergey Bankov for fruitful discussions.

**Disclosures.** The authors declare no conflicts of interest.

See Supplement 1 for supporting content.

#### REFERENCES

1. R. F. Oulton, V. J. Sorger, D. Genov, D. Pile, and X. Zhang, "A hybrid plasmonic waveguide for subwavelength confinement and long-range propagation," *Nat. Photonics* **2**, 496–500 (2008).
2. W. Bogaerts, M. Fiers, and P. Dumon, "Design challenges in silicon photonics," *IEEE J. Sel. Top. Quantum Electron.* **20**, 8202008 (2013).
3. J. Touch, Y. Cao, M. Ziyadi, A. Almain, A. Mohajerin-Ariaei, and A. E. Willner, "Digital optical processing of optical communications: towards an optical turing machine," *Nanophotonics* **6**, 507–530 (2017).
4. D. Thomson, A. Zilkie, J. E. Bowers, T. Komljenovic, G. T. Reed, L. Vivien, D. Marris-Morini, E. Cassan, L. Viro, and J.-M. Fédéli, "Roadmap on silicon photonics," *J. Opt.* **18**, 073003 (2016).
5. M. Skorobogatiy, *Nanostructured and Subwavelength Waveguides: Fundamentals and Applications* (Wiley, 2012).
6. D. A. Miller, "Device requirements for optical interconnects to silicon chips," *Proc. IEEE* **97**, 1166–1185 (2009).
7. M. J. Weber, *Handbook of Optical Materials* (CRC Press, 2018).
8. R. Nagarajan, C. H. Joyner, R. P. Schneider, J. S. Bostak, T. Butrie, A. G. Dentai, V. G. Dominic, P. W. Evans, M. Kato, and M. Kauffman, "Large-scale photonic integrated circuits," *IEEE J. Sel. Top. Quantum Electron.* **11**, 50–65 (2005).
9. C. Yeh and F. I. Shimabukuro, *The Essence of Dielectric Waveguides* (Springer, 2008).

10. L. Chrostowski and M. Hochberg, *Silicon Photonics Design: From Devices to Systems* (Cambridge University, 2015).
11. V. R. Almeida, Q. Xu, C. A. Barrios, and M. Lipson, "Guiding and confining light in void nanostructure," *Opt. Lett.* **29**, 1209–1211 (2004).
12. S. A. Maier, P. G. Kik, H. A. Atwater, S. Meltzer, E. Harel, B. E. Koel, and A. A. Requicha, "Local detection of electromagnetic energy transport below the diffraction limit in metal nanoparticle plasmon waveguides," *Nat. Mater.* **2**, 229–232 (2003).
13. S. I. Bozhevolnyi, V. S. Volkov, E. Devaux, J.-Y. Laluet, and T. W. Ebbesen, "Channel plasmon subwavelength waveguide components including interferometers and ring resonators," *Nature* **440**, 508–511 (2006).
14. N. Engheta, "Circuits with light at nanoscales: optical nanocircuits inspired by metamaterials," *Science* **317**, 1698–1702 (2007).
15. S. A. Maier, *Plasmonics: Fundamentals and Applications* (Springer, 2007).
16. A. A. Maradudin, J. R. Sambles, and W. L. Barnes, *Modern Plasmonics* (Elsevier, 2014), Vol. 4.
17. P. Melentiev, A. Kuzin, V. Balykin, A. Ignatov, and A. Merzlikin, "Dielectric-loaded plasmonic waveguide in the visible spectral range," *Laser Phys. Lett.* **14**, 126201 (2017).
18. P. N. Melentiev, A. Kalmykov, A. Kuzin, D. Negrov, V. Klimov, and V. I. Balykin, "Open-type SPP waveguide with ultra-high-bandwidth up to 3.5 THz," *ACS Photon.* **6**, 1425–1433 (2019).
19. D. Baranov, A. Vinogradov, and A. Lisyansky, "Magneto-optics enhancement with gain-assisted plasmonic subdiffraction chains," *J. Opt. Soc. Am. B* **32**, 281–289 (2015).
20. T. J. Davis, D. E. Gómez, and A. Roberts, "Plasmonic circuits for manipulating optical information," *Nanophotonics* **6**, 543–559 (2016).
21. A. M. Pikalov, A. V. Dorofeenko, and Y. E. Lozovik, "Dispersion relations for plasmons in complex-shaped nanoparticle chains," *Phys. Rev. B* **98**, 085134 (2018).
22. L. Novotny and C. Hafner, "Light propagation in a cylindrical waveguide with a complex, metallic, dielectric function," *Phys. Rev. E* **50**, 4094 (1994).
23. E. Chubchev and A. Vinogradov, "Amplifying of surface plasmon-polariton in a metal-gain medium-vacuum structure," *J. Commun. Technol. Electron.* **62**, 119–122 (2017).
24. E. Chubchev, E. Andrianov, A. Pukhov, A. Vinogradov, and A. Lisyansky, "On correctness of the two-level model for description of active medium in quantum plasmonics," *J. Phys. B* **50**, 175401 (2017).
25. A. Moradi, "Plasmon hybridization in metallic nanotubes," *J. Phys. Chem. Solids* **69**, 2936–2938 (2008).
26. Z. Hashin and S. Shtrikman, "On some variational principles in anisotropic and nonhomogeneous elasticity," *J. Mech. Phys. Solids* **10**, 335–342 (1962).
27. Z. Hashin and S. Shtrikman, "A variational approach to the theory of the elastic behaviour of polycrystals," *J. Mech. Phys. Solids* **10**, 343–352 (1962).
28. D. J. Bergman and D. Stroud, "Physical properties of macroscopically inhomogeneous media," in *Solid State Physics* (Elsevier, 1992), pp. 147–269.
29. P. B. Johnson and R.-W. Christy, "Optical constants of the noble metals," *Phys. Rev. B* **6**, 4370 (1972).
30. A. D. Rakić and M. L. Majewski, "Modeling the optical dielectric function of GaAs and AlAs: extension of Adachi's model," *J. Appl. Phys.* **80**, 5909–5914 (1996).
31. L. A. Vainshtein, *Electromagnetic Waves* (Radio Sviaz, 1988).
32. A. Moradi, "Plasmon hybridization in coated metallic nanowires," *J. Opt. Soc. Am. B* **29**, 625–629 (2012).
33. N. Kirstaedter, O. Schmidt, N. Ledentsov, D. Bimberg, V. Ustinov, A. Y. Egorov, A. Zhukov, M. Maximov, P. Kop'ev, and Z. I. Alferov, "Gain and differential gain of single layer InAs/GaAs quantum dot injection lasers," *Appl. Phys. Lett.* **69**, 1226–1228 (1996).
34. A. Lisyansky, I. Nechepurenko, A. Dorofeenko, A. Vinogradov, and A. Pukhov, "Channel spaser: Coherent excitation of one-dimensional plasmons from quantum dots located along a linear channel," *Physical Review B* **84**, 153409 (2011).
35. Y. Arakawa and A. Yariv, "Quantum well lasers—gain, spectra, dynamics," *IEEE J. Quantum Electron.* **22**, 1887–1899 (1986).
36. Y.-J. Lu, J. Kim, H.-Y. Chen, C. Wu, N. Dabidian, C. E. Sanders, C.-Y. Wang, M.-Y. Lu, B.-H. Li, and X. Qiu, "Plasmonic nanolaser using epitaxially grown silver film," *Science* **337**, 450–453 (2012).
37. E. Lizhev, A. Dorofeenko, L. Huizhe, A. Vinogradov, and S. Zouhdi, "Epsilon-near-zero material as a unique solution to three different approaches to cloaking," *Appl. Phys. A* **100**, 321–325 (2010).
38. I. P. Marko, C. A. Broderick, S. Jin, P. Ludewig, W. Stolz, K. Volz, J. M. Rorison, E. P. O'Reilly, and S. J. Sweeney, "Optical gain in GaAsBi/GaAs quantum well diode lasers," *Sci. Rep.* **6**, 28863 (2016).
39. T. Skauli, P. Kuo, K. Vodopyanov, T. Pinguet, O. Levi, L. Eyres, J. Harris, M. Fejer, B. Gerard, and L. Becouarn, "Improved dispersion relations for GaAs and applications to nonlinear optics," *J. Appl. Phys.* **94**, 6447–6455 (2003).
40. D. Saxena, S. Mokkapatil, P. Parkinson, N. Jiang, Q. Gao, H. H. Tan, and C. Jagadish, "Optically pumped room-temperature GaAs nanowire lasers," *Nat. Photonics* **7**, 963–968 (2013).
41. S. I. Bozhevolnyi, "Plasmonic nano-guides and circuits," in *Plasmonics and Metamaterials* (Optical Society of America, 2008), paper MWD3.
42. E. Chubchev, I. Nechepurenko, A. Dorofeenko, A. Vinogradov, and A. Lisyansky, "Highly confined surface plasmon polaritons in the ultraviolet region," *Opt. Express* **26**, 9050–9062 (2018).
43. E. Chubchev, A. Dorofeenko, and A. Vinogradov, "The influence of a finite size of spheroids forming a chain on the properties of surface plasmons," *J. Commun. Technol. Electron.* **63**, 850–857 (2018).